

# Is osteoporosis systemic?

Ronald L. Huston<sup>1</sup>, Kenneth L. Weiss<sup>2</sup>, Rutvij Kotecha<sup>3</sup>, Mina Dimov<sup>1</sup>

<sup>1</sup>School of Dynamic Systems, University of Cincinnati, Cincinnati, USA

<sup>2</sup>Neuroimaging Research and Radiology, University of Mississippi Medical Center, Jackson, USA

<sup>3</sup>Material Science and Engineering, University of Cincinnati, Cincinnati, USA

Email: [ron.huston@uc.edu](mailto:ron.huston@uc.edu)

Received 21 January 2013; revised 3 March 2013; accepted 5 April 2013

Copyright © 2013 Ronald L. Huston *et al.* This is an open access article distributed under the Creative Commons Attribution License, which permits unrestricted use, distribution, and reproduction in any medium, provided the original work is properly cited.

## ABSTRACT

**The title question is investigated by comparing results of a series of bone strength tests of lumbar vertebrae (L1 and L2) and right wrists (distal radii) of nine cadavers. The paper describes the specimen preparation, the testing, and the analysis procedures. The results show that there is a correlation between the strengths of the lumbar and wrist specimens for the individual cadavers, suggesting that bone integrity is indeed systemic.**

**Keywords:** Osteoporosis; Bone Mineral Density; Bone Fracture; Bone Strength

## 1. INTRODUCTION

At an NIH conference in 2000, osteoporosis was defined as: “a skeletal disorder characterized by compromised bone strength predisposing to an increased risk of fracture” [1].

In a relatively recent report (2011) the US Preventive Services Task Force (USPSTF) [2] estimated that 12 million Americans currently have osteoporosis and that “half of all post-menopausal women will have an osteoporosis-related fracture during their lifetime.”

The excessive cost of this widespread disease includes not only treatment but also the cost of diagnosis. Currently firm diagnosis typically occurs after a bone fracture via X-ray or MRI imaging of the large bones. However, if diagnosis could be made simpler and sooner, the cost of diagnosis could be reduced and preventive measures (e.g. Diet/exercise as discussed by Dimov (2010)) could be taken [3].

If osteoporosis is systemic, as opposed to being localized in large bones and vertebrae, then using advanced imaging techniques, diagnosis using extremities is feasible. Indeed, Oyen *et al.* (2010) [4] discovered in a recent

study that 1/3 to 1/2 of elderly persons (over age 50) with low-energy distal radius fracture have low bone mineral density (BMD).

*In vivo* MRI studies show that micro MRI imaging can detect architectural changes in trabecular bone of the distal radii. These changes are believed to be good biomarkers for osteoporosis. That is, if a systemic nature of osteoporosis can be established, technical advances in imaging can be used for early osteoporosis diagnosis.

To test the systemic hypothesis, we physically measured and compared the bone strengths of lumbar vertebrae and distal radii of nine cadavers with varying degrees of low bone mineral densities. The results suggest a strong correlation between the strengths of the vertebrae and the radii for individual cadavers.

The balance of the paper is divided into five parts with the first part describing the physical testing, which is then followed by listings of measurement and testing results. The next two parts provide an analysis of the data and subsequent computed results. The final part is a discussion with concluding remarks.

## 2. PHYSICAL TESTING

### 2.1. Vertebrae

Once harvested the lumbar vertebrae (L1 and L2) were cut through the discs so that the specimens then had flat superior and inferior surfaces. Also, the spinous processes were removed resulting in specimens in the form of short cylinders having curved perimeters as depicted in **Figure 1**, where the principal dimensions are shown.

We used a dial caliper to measure the five dimensions of **Figure 1** for the 18 specimens used in the testing (9 L1 and 9 L2).

After taking these measurements we placed the specimens in shallow plastic flat-dishes containing a liquid cold-curing resin. Upon hardening the specimens were inverted and the other end (superior end) was placed in

hardening resin dishes with care taken to keep the superior/inferior dish surfaces parallel. **Figure 2** shows a sketch of the resulting vertebral specimen constructs.

Next, we placed each of the 18 constructs in an Instron tester and compressed them to failure (large displacement with minimal load increase). During the compression we recorded the load/displacement values up to failure and then the failure load itself.

### 2.2. Right Distal Radii

As with the vertebrae, the distal radii (once harvested) were cut perpendicular to their axes with the proximal and distal cutting planes being parallel. The bone tissue in the cross-sections was found to be near annular ellipses as represented in **Figure 3**, where the pertinent dimensions are also show. The specimens then have the approximate shape of a truncated annular elliptical conical segment.

Next, we placed the nine radii constructs in the Instron machine and compressed them to failure. As with the vertebrae, we recorded the load/displacement values up to failure and then the failure load itself.

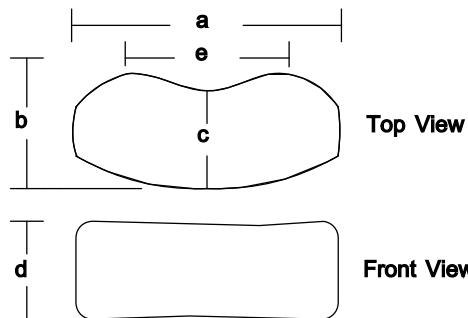


**Figure 1.** Geometry of vertebral specimens.



**Figure 2.** Vertebral test construct.

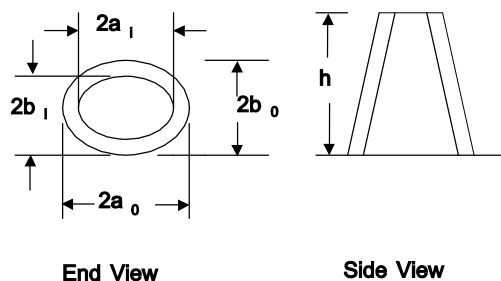


**Figure 3.** Distal radii wrist bone geometry.

## 3. MEASUREMENT AND TESTING RESULTS

### 3.1. Vertebrae

**Table 1** lists the measurements of the geometric parameters shown in **Figure 1** for the L1 and L2 vertebrae.

**Table 2** lists the failure loads and the slopes of the nearly linear load/displacement relations obtained during the compression testings, for all 18 vertebral specimens.

### 3.2. Right Distal Radii

**Tables 3** and **4** list the measurements of the parameters of **Figure 3** for the distal and proximal ends of the right radii specimens, and also in **Table 4** the specimen lengths.

Finally, **Table 5** lists the failure loads and the slopes of the nearly linear load/displacement relations obtained during compression testing.

## 4. ANALYSIS

### 4.1. Vertebrae

To determine the vertebral strengths we needed to know their cross-section areas. To this end we used the geometry represented in **Figure 1** together with the measured data listed in **Table 1**. To facilitate this we divided the vertebral cross-section region into three parts as in **Figure 4** with circle segments representing the ends and the central region being a near rectangle.

Using standard handbook mensuration formulas [4] for the segment areas we were able to estimate the vertebral cross-section areas in terms of the measured dimensions of **Figure 3**. From the summary analysis of the Appendix we obtained the following area algorithm:

Let  $t$  be defined as:

$$t = (a - e) / 2 \tag{1}$$

Next, let  $r$  be defined as:

$$r = \left( \frac{b^2}{8t} \right) + (t/2) \tag{2}$$

Then the cross-section area  $A$  of a vertebral specimen is approximately:

$$A = ec + r^2 \cos^{-1} \left( \frac{r-t}{r} \right) - (r-t)(2rt - t^2)^{1/2} \tag{3}$$

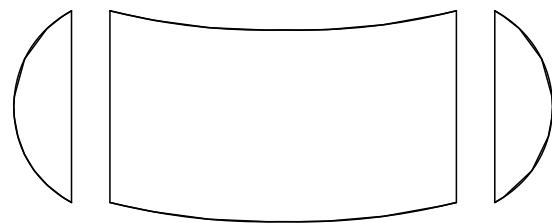


**Figure 4.** Segmentation of a vertebral cross-section area.

**Table 1.** Vertebral geometric measurements<sup>1</sup> (see **Figure 1**).

Vertebral Label	A	B	C	D	E
CC-L1	2.014 (51.56)	1.552 (39.42)	1.438 (36.52)	1.399 (35.53)	1.100 (27.94)
CC-L2	2.232 (56.69)	1.606 (40.79)	1.584 (40.23)	1.483 (37.67)	1.175 (29.84)
HH-L1	1.678 (42.62)	1.505 (38.23)	1.452 (36.88)	1.116 (28.35)	1.050 (26.67)
HH-L2	2.062 (52.37)	1.599 (40.61)	1.471 (37.36)	1.117 (28.37)	1.103 (28.02)
II-L1	1.775 (45.08)	1.320 (33.07)	1.295 (32.89)	1.438 (36.52)	1.250 (31.75)
II-L2	1.788 (45.41)	1.531 (38.89)	1.455 (36.96)	1.459 (37.06)	1.005 (25.53)
JJ-L1	2.104 (53.44)	1.566 (39.78)	1.357 (34.47)	1.476 (37.54)	1.130 (28.70)
JJ-L2	2.106 (53.49)	1.445 (36.70)	1.445 (36.70)	1.826 (46.38)	1.416 (35.97)
MM-L1	1.694 (43.03)	1.238 (31.44)	1.174 (29.82)	1.069 (27.15)	1.050 (26.67)
MM-L2	1.696 (41.88)	1.244 (31.60)	1.214 (30.84)	1.173 (29.79)	1.186 (30.12)
NN-L1	2.096 (53.24)	1.384 (35.15)	1.188 (30.18)	1.547 (39.29)	1.000 (25.40)
NN-L2	2.001 (50.82)	1.418 (36.02)	1.430 (36.32)	1.339 (34.01)	1.081 (27.30)
EEE-L1	2.205 (56.01)	1.684 (42.77)	1.629 (41.38)	1.702 (43.23)	1.500 (38.10)
EEE-L2	2.395 (60.83)	1.727 (43.87)	1.655 (42.04)	1.665 (42.29)	1.075 (27.30)
HHH-L1	1.629 (41.38)	1.281 (32.54)	1.214 (30.84)	1.095 (27.81)	1.175 (29.84)
HHH-L2	1.984 (50.39)	1.407 (35.74)	1.326 (33.68)	1.530 (38.18)	1.135 (28.83)
JJJ-L1	1.981 (50.32)	1.281 (32.54)	1.284 (32.61)	1.449 (36.80)	1.132 (28.75)
JJJ-L2	1.930 (49.02)	1.435 (36.45)	1.380 (35.05)	1.477 (37.52)	1.134 (28.80)

<sup>1</sup>Measurements are in inches (in) with millimeters (mm) in parentheses.

**Table 2.** Failure loads and stiffnesses of the 18 vertebral constructs.

Vertebral Label	Failure Loads <sup>1</sup>		Stiffnesses <sup>2</sup> (Load/Displacement) k	
	L1	L2	L1	L2
CC	1329 (6.089)	2050 (9.118)	19200 (3361.9)	50000 (8755.0)
HH	375 (1.668)	1191 (5.298)	9400 (1120.6)	42393 (7423.0)
II	1352 (6.014)	1983 (8.820)	20797 (3641.6)	41667 (7295.9)
JJ	1978 (8.798)	1909 (8.491)	45456 (7959.3)	34286 (6003.5)
MM	419 (1.864)	856 (3.807)	7017 (1229.7)	28571 (5002.8)
NN	674 (2.998)	2099 (9.336)	7778 (1361.9)	56250 (9849.4)
EEE	1029 (4.799)	3823 (17.004)	10948 (1917.0)	28571 (5002.8)
HHH	474 (2.108)	1123 (4.995)	13159 (2304.1)	17281 (3025.9)
JJJ	1479 (6.578)	2277 (10.128)	32000 (5603.2)	30000 (5253.0)

<sup>1</sup>Loads are in pounds (lb) with kiloNewtons (kN) in parentheses. <sup>2</sup>Stiffnesses are in pounds per inch (lb/in) with kiloNewton per meter (kN/m) in parentheses.

where a, b, c, and e are shown in **Figure 1**. Once we have values for the cross-section areas, we can readily determine the specimen strength using elementary strength of materials formulas: Specifically, for a uniform cross-section member with length  $\ell$  and cross-section area A, and subjected to a compressive load P as in **Figure 5**, the

shortening  $\delta$  of the member is simply:

$$\delta = P\ell/AE \quad (4)$$

where E is the elastic modulus (see Beer and Johnston [6]).

The stress and the strain  $\epsilon$  are then defined as

**Table 3.** Distal end geometric measurements\*.

Radius Label	2a <sub>od</sub>	2b <sub>od</sub>	2a <sub>id</sub>	2b <sub>id</sub>
CC	0.870 (22.098)	0.640 (16.256)	0.656 (16.662)	0.455 (11.557)
HH	0.680 (17.272)	0.400 (10.160)	0.487 (12.370)	0.245 (6.223)
II	0.652 (16.561)	0.417 (10.592)	0.428 (10.871)	0.248 (6.299)
JJ	0.938 (23.852)	0.540 (13.716)	0.735 (18.669)	0.341 (8.661)
MM	0.685 (17.399)	0.467 (11.862)	0.493 (12.528)	0.338 (8.585)
NN	0.685 (17.399)	0.446 (11.328)	0.453 (11.506)	0.283 (7.188)
EEE	0.846 (21.488)	0.528 (13.411)	0.609 (15.469)	0.306 (7.772)
HHH	0.641 (16.281)	0.385 (9.779)	0.464 (11.786)	0.260 (6.604)
JJJ	0.715 (18.161)	0.499 (12.675)	0.557 (14.148)	0.295 (7.493)

\*Subscripts d for distal Measurements are in inches (in) with millimeters (mm) in parentheses.

**Table 4.** Proximal end geometric measurements\* (see Figure 3).

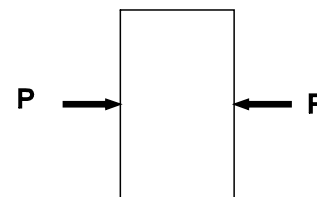
Radius Label	2a <sub>op</sub>	2b <sub>op</sub>	2a <sub>ip</sub>	2b <sub>ip</sub>	H
CC	0.775 (19.685)	0.590 (14.986)	0.410 (10.414)	0.295 (7.493)	1.197 (30.404)
HH	0.551 (13.995)	0.371 (9.423)	0.311 (7.899)	0.180 (4.572)	1.164 (29.566)
II	0.590 (14.986)	0.394 (10.008)	0.308 (7.823)	0.291 (7.391)	0.936 (23.774)
JJ	0.847 (21.514)	0.503 (12.776)	0.567 (14.402)	0.320 (8.128)	0.902 (22.911)
MM	0.587 (14.910)	0.430 (10.922)	0.403 (10.236)	0.289 (7.341)	1.129 (28.677)
NN	0.614 (15.596)	0.437 (12.370)	0.289 (7.341)	0.204 (5.182)	1.094 (27.788)
EEE	0.684 (17.377)	0.467 (11.862)	0.391 (9.931)	0.206 (5.232)	0.999 (25.375)
HHH	0.512 (13.005)	0.363 (9.220)	0.252 (6.401)	0.182 (4.623)	1.288 (32.715)
JJJ	0.573 (14.554)	0.441 (11.201)	0.291 (7.391)	0.194 (4.928)	1.121 (28.473)

\*Subscripts p for proximal. Measurements are in inches (in) with millimeters (mm) in parentheses.

**Table 5.** Failure loads and stiffnesses of the 9 right radii (wrist) constructs.

Radius Label	Failure Loads <sup>1</sup>	Stiffnesses <sup>2</sup> (load/displacement) k
CC	167.36 (0.700)	149.4 (26.163)
HH	74.18 (0.330)	82.0 (14.360)
II	83.18 (0.370)	109.3 (19.140)
JJ	138.25 (0.615)	110.2 (19.298)
MM	73.06 (0.315)	94.5 (16.549)
NN	179.84 (0.800)	158.7 (27.791)
EEE	221.12 (0.984)	148.5 (26.005)
HHH	61.82 (0.275)	87.5 (15.323)
JJJ	224.80 (1.000)	239.7 (41.975)

<sup>1</sup>Loads are in pounds (lb) with kiloNewtons (kN) in parentheses. <sup>2</sup>Stiffnesses are in pounds per inch (lb/in) with kiloNewtons per meter (kN/m) in parentheses.

**Figure 5.** A specimen in compression.

$$\sigma = P/A \quad \text{and} \quad \varepsilon = \delta/\ell \quad (5)$$

with the “strength” being the maximum stress value  $\sigma_{\max}$  occurring at the failure load  $P_{\max}$ , or at the collapse of the specimen member.

The elastic modulus  $E$  is a measure of the stiffness of the specimen. It is simply the slope  $k$  of the linear portion of a graphical representation between the stress  $\sigma$  and the strain  $\varepsilon$ , or equivalently, between the load  $P$  and the displacement  $\delta$ . That is, from Eqs.4 and 5 we have

$$\sigma = E\varepsilon \text{ or } E = \Delta\sigma/\Delta\varepsilon = (\ell/A)\Delta P/\Delta\delta = k\ell/A \quad (6)$$

Where  $\Delta$  is a finite difference.

The strength  $\sigma_{max}$  and the stiffness E are thus measures of the structural integrity of the vertebral specimens and thus can be used for comparison evaluations.

#### 4.2. Distal Radii

As with the vertebrae, we also needed the cross-section areas of the distal radii, to evaluate their strengths. To this end, consider again the sketch of the distal radii bone specimens shown in **Figure 3**. Although the specimens have a longitudinal taper, the measurements recorded in **Tables 4** and **5** show that the taper is slight, so that for deformation and stress calculations it is reasonable to simply assume a linear cross-section area change.

The bone content of the radii cross-sections are nearly annular ellipses. Therefore, with an ellipse area being:  $\pi ab$ , with a and b being semi-major and semi-minor axes, the distal and proximal cross-section areas are:

$$\begin{aligned} A_d &= \pi(a_{d_o} b_{d_o} - a_{d_i} b_{d_i}), \\ A_p &= \pi(a_{p_o} b_{p_o} - a_{p_i} b_{p_i}) \end{aligned} \quad (7)$$

The average bone cross-section is then

$$A_{avg} = (A_d + A_p)/2 \quad (8)$$

Consider again the side view of the radius specimen as in **Figure 3** and as shown again in **Figure 6** identifying the end areas and with an axial coordinate y. Then we see that the cross-section area A(y) along the axis of the specimen is:

$$A(y) = A_d + (A_p - A_d)(y/h) \quad (9)$$

Beer and Johnston [6] state that the shortening  $\delta$  of the tapered specimen is given by the formula:

$$\delta = \int_0^h \frac{Pdy}{AE} \quad (10)$$

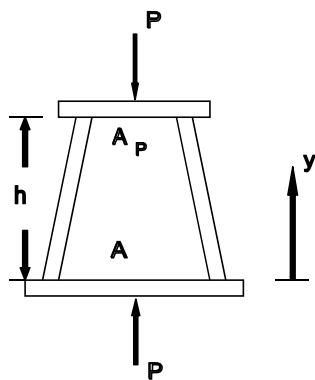


**Figure 6.** Distal radii wrist specimen geometry.

By substituting for A from **Eq.9** we find  $\delta$  to be:

$$\delta = \frac{Ph}{E(A_d - A_p)} \ln(A_d/A_p) \quad (11)$$

In the course of the loading of the specimen (before collapse) we found the loading and the deformation to be linearly related. That is,

$$P = k\delta \quad (12)$$

where, as with the vertebrae, the stiffness constant k may be identified as the slope of the newly linear load/displacement relation.

### 5. COMPUTED RESULTS

#### 5.1. Vertebrae

**Table 6** lists the cross-section areas of the L1 and L2 specimens, calculated using the formulas of **Eqs.1-3**, and the resulting strengths and elastic moduli.

We used the failure load data of **Table 2** and the computed areas to obtain the strengths of the vertebrae. Also, by using the stiffnesses listed in **Table 2** we obtained the elastic moduli using **Eq.6**.

#### 5.2. Distal Radii

The radii strengths and elastic moduli can be computed using the failure loads and stiffness values listed in **Table 6**, the measured geometric dimensions of **Tables 3** and **4**, and then **Eqs.7, 8** and **13**, to determine the numerical results. To this end, it is helpful to initially determine the cross-section area parameters of **Eqs.8** and **13**.

In view of **Eq.8**, it is helpful to compute some area ratios needed for determining the elastic modulus. Also, it is useful to have the product of the construct height h (see **Figure 3**) and the stiffness k of **Table 5**. To this end **Table 7** lists the distal, proximal and average areas and area ratios and stiffness-height products of the bone content of the various radii.

Finally, using failure loads listed in **Table 5** and the parameters of **Table 7**, we obtain the radii strengths and elastic moduli as listed in **Table 8**.

### 6. DISCUSSION AND CONCLUSIONS

**Table 9** summarizes the foregoing results providing a comparison between the strengths of the specimen constructs from the three sites. A glance at the results shows the general trend that there is a correlation between the strengths of the distal radii and the vertebrae for the corresponding cadavers. There is an especially strong correlation between the radii and the L2 vertebrae.

Observe also in **Table 9** that the strengths of the wrist radii are generally higher than those for the vertebrae.

**Table 6.** Vertebral construct cross-section areas, strengths, and elastic moduli.

Vertebral Label	Cross-Section Areas			
	L1		L2	
CC	2.580 (16.645)		3.220 (20.774)	
HH	2.175 (14.032)		2.713 (17.503)	
II	2.095 (13.516)		2.302 (14.852)	
JJ	2.625 (16.935)		2.740 (17.677)	
MM	1.792 (11.561)		1.949 (12.574)	
NN	2.317 (14.948)		2.967 (19.142)	
EEE	3.262 (21.045)		3.464 (22.348)	
HHH	1.824 (11.768)		2.358 (15.213)	
JJJ	2.125 (13.710)		2.372 (15.303)	
Vertebral Label	Strengths		Elastic Moduli	
	L1	L2	L1	L2
CC	515.1 (3.552)	637 (4.392)	8551 (58.959)	23050 (158.93)
HH	172.4 (1.189)	439 (3.027)	3583 (24.704)	17466 (120.43)
II	645.3 (4.449)	861 (5.937)	12399 (85.491)	26417 (182.14)
JJ	753.5 (5.195)	697 (4.806)	20659 (142.44)	22834 (157.44)
MM	233.8 (1.612)	439 (3.027)	3422 (23.594)	17200 (118.59)
NN	290.9 (2.006)	707 (4.874)	4381 (3.0200)	25369 (174.92)
EEE	315.5 (2.175)	1104 (7.612)	5886 (40.584)	13743 (94.758)
HHH	259.9 (1.792)	476 (3.282)	6154 (42.432)	11215 (79.327)
JJJ	696.0 (4.799)	960 (6.619)	6788 (46.803)	18690 (128.87)

Values are in square inches (in<sup>2</sup>) with square centimeters (cm<sup>2</sup>) in parentheses, and in pounds per square inch (psi) with mega Pascals (mPa) in parentheses.

**Table 7.** Cross-section areas of distal radii bone, area ratios and stiffness-height products.

Radius Label	Proximal End A <sub>p</sub> *	Distal End A <sub>d</sub> *	Average A <sub>ave</sub> *	
CC	0.264 (1.703)	0.203 (1.310)	0.234 (1.510)	
HH	0.116 (0.748)	0.120 (0.774)	0.118 (0.761)	
II	0.112 (0.723)	0.130 (0.839)	0.121 (0.781)	
JJ	0.192 (1.239)	0.200 (1.290)	0.196 (1.265)	
MM	0.107 (0.690)	0.120 (0.774)	0.114 (0.735)	
NN	0.164 (1.058)	0.139 (0.897)	0.152 (0.981)	
EEE	0.187 (1.206)	0.205 (1.323)	0.196 (1.264)	
HHH	0.110 (0.710)	0.090 (0.581)	0.100 (0.645)	
JJJ	0.155 (1.000)	0.152 (0.981)	0.153 (0.987)	
Radius Label	A <sub>p</sub> /A <sub>d</sub>	ln(A <sub>p</sub> /A <sub>d</sub> )	$\frac{\ln(A_p/A_d)}{A_p - A_d}$ **	kh***
CC	1.297	0.2604	4.304	178.83
HH	0.967	-0.0338	8.460	95.45
II	0.855	-0.1566	8.286	102.30
JJ	0.960	-0.0402	5.094	99.40
MM	0.889	-0.118	8.821	106.69
NN	1.177	0.1631	6.603	173.62
EEE	0.914	-0.090	5.102	148.35
HHH	1.222	0.201	10.034	112.70
JJJ	1.204	0.020	6.516	268.70

\*Values are in square inches (in<sup>2</sup>) with square centimeters (cm<sup>2</sup>) in parentheses; \*\*Units in reciprocal square inches (in<sup>-2</sup>); \*\*\*Units in pounds.

**Table 8.** Strengths and elastic moduli for the distal radii.

Radius Label	Strength	Elastic Modulus
CC	672.5 (4.636)	770 (5.308)
HH	628.6 (4.333)	808 (5.570)
II	687.4 (4.739)	848 (5.846)
JJ	705.4 (4.863)	506 (3.488)
MM	640.9 (4.418)	941 (6.487)
NN	1883.2 (8.156)	1146 (7.900)
EEE	1128.2 (7.776)	757 (5.219)
HHH	618.2 (4.262)	1133 (7.797)
JJJ	1469.3 (10.129)	1751 (12.071)

Values are in pounds per square inch (psi) with megaPascals (mPa) in parentheses.

**Table 9.** Strength comparisons for the three construct.

Construct Label	L1	L2	Wrist Radii
CC	515.1 (3.552)	637 (4.392)	672.5 (4.636)
HH	172.4 (1.189)	439 (3.027)	628.6 (4.333)
II	645.3 (4.449)	861 (5.937)	687.4 (4.739)
JJ	753.5 (5.195)	697 (4.806)	705.4 (4.863)
MM	233.8 (1.612)	439 (3.027)	640.9 (4.418)
NN	290.9 (2.006)	707 (4.874)	1183.2 (8.156)
EEE	315.5 (2.175)	1104 (7.612)	1128.3 (7.776)
HHH	259.9 (1.792)	476 (3.282)	618.2 (4.262)
JJJ	696.0 (4.799)	960 (6.619)	1469.3 (10.129)

Values are in pounds per square inch (psi) with megaPascals (mPa) in parentheses.

This is to be expected since the radii bone is cortical whereas the vertebrae have load sharing between cortical and trabecular bone. Eswaran, *et al.* (2006) [7] discuss this effect in detail.

## 7. ACKNOWLEDGEMENTS

The authors acknowledge and appreciate the assistance of Richard Banto, Dale Weber, Y. Su, Susan Neuman, and Linda Levin.

## REFERENCES

- [1] National Institutes of Health (2000) NIH consensus development conference on osteoporosis.
- [2] US Preventive Services Task Force (2011) Screening for osteoporosis: Recommendation statement. *American Family Physician*, **83**, 1197-1200.
- [3] Dimov, M., Khoury, J.D. and Tsang, R.C. (2010) Bone mineral loss during pregnancy: Is tennis protective? *Journal of Physical Activity & Health*, **7**, 239-245.
- [4] Oyen, J., Gjesdal, C.G., Brudvik, C., Hove, L.M., Apalset, E.M., Sulseth, H.C. and Hangeberg, G. (2010) Low-energy distal radius fractures in middle-aged and elderly men and women—The burden of osteoporosis and fracture risk—A study of 1794 consecutive patients. *Osteoporosis International*, **21**, 1257-1267.
- [5] Selby, S.M. (1972) CRC standard mathematical tables. 20th Edition, The Chemical Rubber Co., Cleveland. [doi:10.1007/s00198-009-1068-x](https://doi.org/10.1007/s00198-009-1068-x)
- [6] Beer, F.P. and Johnston Jr., E.R. (1992) Mechanics of materials. 2nd Edition, McGraw-Hill, New York.
- [7] Eswaran, S.K., Gupta, A., Adams, M.F. and Keaveny, T.M. (2006) Cortical and trabecular load sharing in the human vertebral body. *Journal of Bone and Mineral Research*, **21**, 307-313. [doi:10.1359/jbmr.2006.21.2.307](https://doi.org/10.1359/jbmr.2006.21.2.307)

**APPENDIX**

To establish a basis for **Eqs.1-3**, consider the circle segment in **Figure A**. From Reference [5] and/or other handbooks, the area  $K$  of the shaded region is:

$$K = r^2 \cos^{-1}\left(\frac{r-t}{r}\right) - (r-t)(2rt - t^2)^{1/2} \quad (A1)$$

In view of the dimensions  $a, \dots, e$  of **Figure A**, we immediately see that  $t$  and  $m$  are

$$t = (a - e)/2, m = b \quad (A2)$$

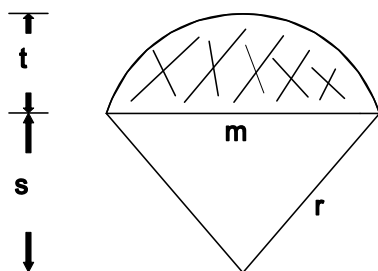


**Figure A.** Circle segment.

Also from [5]  $m, t,$  and  $r$  are related to each other by the expression:

$$m^2 = 4t(2r - t) \quad (A3)$$

By solving for  $r$  we have

$$r = (m^2/8t) + (t/2) \quad (A4)$$

Referring again to **Figure 1** and also to **Figure 4** we see that the cross section areas  $A$  of the vertebral specimens may be represented as:

$$A = ec + K \quad (A5)$$

or

$$A = ec + r^2 \cos^{-1}\left(\frac{r-t}{r}\right) - (r-t)(2rt - t^2)^{1/2} \quad (A6)$$

**Eqs.A2, A4,** and **A6** form the basis for the algorithm of Equations.